Hindawi
Advances in Civil Engineering
Volume 2019, Article ID 6572465, 15 pages
https://doi.org/10.1155/2019/6572465

Research Article

Seismic Performance Evaluation of Modern Bare and Masonry-Infilled RC SMRF Structures

M. E. Ahmad, N. Ahmad, S. Pervez, A. Iqbal, A. Z. Khan, M. E. Rahim, W. Hassan, K. Umer, and K. Khan

Department of Civil Engineering, UET Peshawar, Peshawar, KP, Pakistan

Correspondence should be addressed to N. Ahmad; naveed.ahmad@uetpeshawar.edu.pk

Received 30 July 2019; Revised 12 August 2019; Accepted 30 August 2019; Published 30 October 2019

Guest Editor: André Furtado

Improper execution of modern code-designed structures in many developing countries have resulted in significant deficient building stock; low strength of concrete, reduced reinforcement, inappropriate detailing of beam-column members, and lack of lateral ties in joint panels. Observations based on earthquake-induced damages and experimental studies conducted on such buildings have revealed significant vulnerability of beam-column joints of bare moment-resisting frame structures. Shake table tests were conducted on selected three 1 : 4 reduced-scale three-story reinforced concrete (RC) moment-resisting frames, including one bare RC frame and two masonry-infilled RC frames, having relatively lower bay width-to-height ratio. The models were tested under multilevels of seismic excitations using natural acceleration time history of 1994 Northridge and also free vibration tests, to acquire the models' dynamic characteristics, i.e., frequencies and elastic viscous damping, and seismic response parameters, i.e., roof displacement, interstory drift and interstory shear, and seismic response curves, in order to understand the role of masonry infill in the selected frames under moderate seismic actions. The inclusion of masonry infill avoided joint shear hinging of the frame. Additionally, the infill provided energy dissipation to the structure through masonry sliding over multiple cracks. This enabled the structure to control seismic displacement demand and resist relatively higher ground motions, yet limiting structural damages.

1. Introduction

The damaged buildings and the resulting casualties observed in majority of the past earthquakes have provided ample evidence that the existing deficient reinforced concrete buildings, those nonconforming to modern seismic codes, are vulnerable against earthquake-imposed actions [1–6]. These observations have revealed that substandard materials (low-strength concrete, reduced size, and low-quality rebars), reduced reinforcement and improper detailing, inadequate anchorage of beam reinforcement in joints, and joints lacking confining ties are major factors causing damage and early collapse of buildings under seismic excitations. Despite the modern nature of reinforced concrete constructions, execution of specified designs in the field still remains a challenge in many developing countries. This has resulted in significant construction deficiencies in the existing building stock. Such vulnerable building stock constitutes a life-safety risk that must be reduced for future earthquakes to avoid socioeconomic disruption. It is worth mentioning that a significant fraction of these structures do not have to be completely replaced; instead, cost-effective rehabilitation techniques can be utilized for seismic upgradation of existing structures [7–19].

Earthquakes always cause damage to deficient RC frame structures in a more complex manner, unlike the more desirable plastic mechanisms observed in code-conforming structures. Most of the time, computation of dynamic properties of deficient structures using simplified analytical procedures is not very accurate, although sufficiently accurate for code-conforming models. The purpose of this research is to understand the seismic behavior of deficient RC special moment-resisting frame (SMRF) structures subjected to seismic excitations, obtain elastic dynamic

properties of considered structures through free vibration tests, and comprehend the role of masonry infill in limiting structural damages in deficient moment-resisting frame structures.

Shake table tests were conducted on a three-story RC bare frame having weaker beam-column joints, which is representative of modern frame structures found in developing countries, and two three-story masonry-infilled RC frames, with the aim to study the effect of masonry infill in improving the seismic behavior of RC moment-resisting frame structures and, further, to obtain the models' seismic response parameters.

2. Experimental Program

2.1. Description of Test Models. Three-story one-bay by one-bay frame structures were considered for investigation, including an RC bare frame and two masonry-infilled RC frames (Figure 1). A frame with relatively lower bay width-to-height aspect ratio was considered. The beams have a cross section of 24 inch × 15 inch (610 mm × 381 mm) and clear length of 9.50 feet (289.56 cm) and 13.50 feet (411.48 cm) in the N-S and E-W directions, respectively. The columns have a cross section of 15 inch × 15 inch (381 mm × 381 mm) and an interstory height of 9.0 feet (274.32 cm). The frame also included infills of solid brick masonry having thickness of 9 inch (228.60 mm). The structural frame was analyzed using the lateral static force procedure given in the BCP-SP [20] for highest seismic hazard zones, which refers to seismic Zone 4 (PGA = 0.40 g), and designed to the ACI-318 [21] recommendations for SMRF structure. The structure design was carried out in the finite element-based software ETABS CSI [22], considering all the load combinations for dead, live, and earthquake loads given in the BCP-SP [20] for commercial and public buildings. Concrete with a compressive strength of 3000 psi (21 MPa) and steel rebars with an yield strength of 60,000 psi (414 MPa) were considered in the design.

In the test model construction, lateral ties were not provided in the beam-column joints, which is a common construction deficiency observed in recent SMRF structures in most of the developing countries [23]. Additionally, concrete with a compressive strength of 2500 psi (17.24 MPa) was used, and longitudinal reinforcement ratio of beam was reduced by 25%. Furthermore, due to the introduction of confined masonry construction technique in the region, the construction sequence of masonry-infilled RC frames has been modified. The present research considered the conventional masonry-infilled RC frame that involved the construction of bare frame, which was then provided with masonry infill. Additionally, a *hybrid* masonry-infilled RC frame was considered, which involved the construction of RC columns, followed by the construction of masonry infill. In the later construction, beams and slabs were casted simultaneously after the masonry infill construction is completed. The beams in this construction are directly placed on the top of masonry infill. Masonry panels in the latter acts like a loadbearing walls since it is carrying both gravity and lateral loads.

2.2. Testing of Masonry-Infill Constituent Materials and Subassemblies. Basic tests were conducted on masonry constituent materials for the estimation of mechanical properties of masonry infill. Figure 2 shows the reduced scale masonry brick unit and wallettes prepared for basic testing. These included tests on brick units, mortar, masonry prisms, and masonry wallettes. Mechanical properties such as compressive strength, in-plane shear, and diagonal tensile strength were determined. The tests were performed according to the standard testing procedures, given as follows: ASTM C-67-06 for testing of masonry units, ASTM C109/C109M-08 for testing of mortar cubes, ASTM C-1314-07 for testing of masonry prisms, and E-519-02 and RILUM LUM B6 for testing of masonry wallettes. Table 1 reports the basic mechanical properties of masonry used for infill in test structures.

2.3. Shake Table Testing of 1 : 4 Reduced-Scale Models

2.3.1. Construction of 1 : 4 Reduced-Scale Test Models. Simple model idealization was adopted to construct 1 : 4 reduced-scale test models. The models' linear dimensions were reduced by a scale factor $S_L = 4.0$. However, the mechanical properties of constituent materials (i.e., rebars, concrete, and masonry) remained the same. Concrete for the 1 : 4 reduced-scale model was prepared with a mix proportion of cement, sand, and 3/8 inch (9 mm) down coarse aggregate. This takes into account the aggregate scaling requirements, and also, achieves the desired concrete strength of 2500 psi (17.24 MPa). A supplemental mass of 400 kg per floor was added to cause significant nonlinearity in the bare frame model subjected to seismic excitations. Tables 2 and 3 report various properties of the designed prototype models and its corresponding reduced scale model. Concrete strength and number of rebars in beam-column members were reduced in the test models in order to take into account the construction deficiencies as observed in the field. The model-to-prototype conversion factors are also listed, which are essential to convert the measured quantities of the reduced-scale model to the corresponding prototype model.

2.3.2. Input Excitations and Test Model Instrumentation Plan. The models were tested using natural acceleration time history for base excitation and free vibration tests. A natural acceleration time history of 1994 Northridge earthquake, particularly the horizontal component recorded at 090 CDMG Station 24278, was extracted from the PEER strong motions database (Figure 3). This record was selected after careful analysis of the number of accelerograms for earthquakes generated by reverse faulting. This record has a maximum acceleration of 0.57 g, maximum velocity of 518 mm/sec, and maximum displacement of 90 mm. The accelerogram time step was reduced by a scale factor of $\sqrt{4}$, shrinking the time duration required for model excitation. The input acceleration of the model was linearly scaled using scaling factors from 0.05 to 2.5 times in order to scale the amplitude of input acceleration to multilevels. The input acceleration amplitude multiplied by a scale factor of 1.0 and 2.50 are referred as NR1 and NR2, respectively.

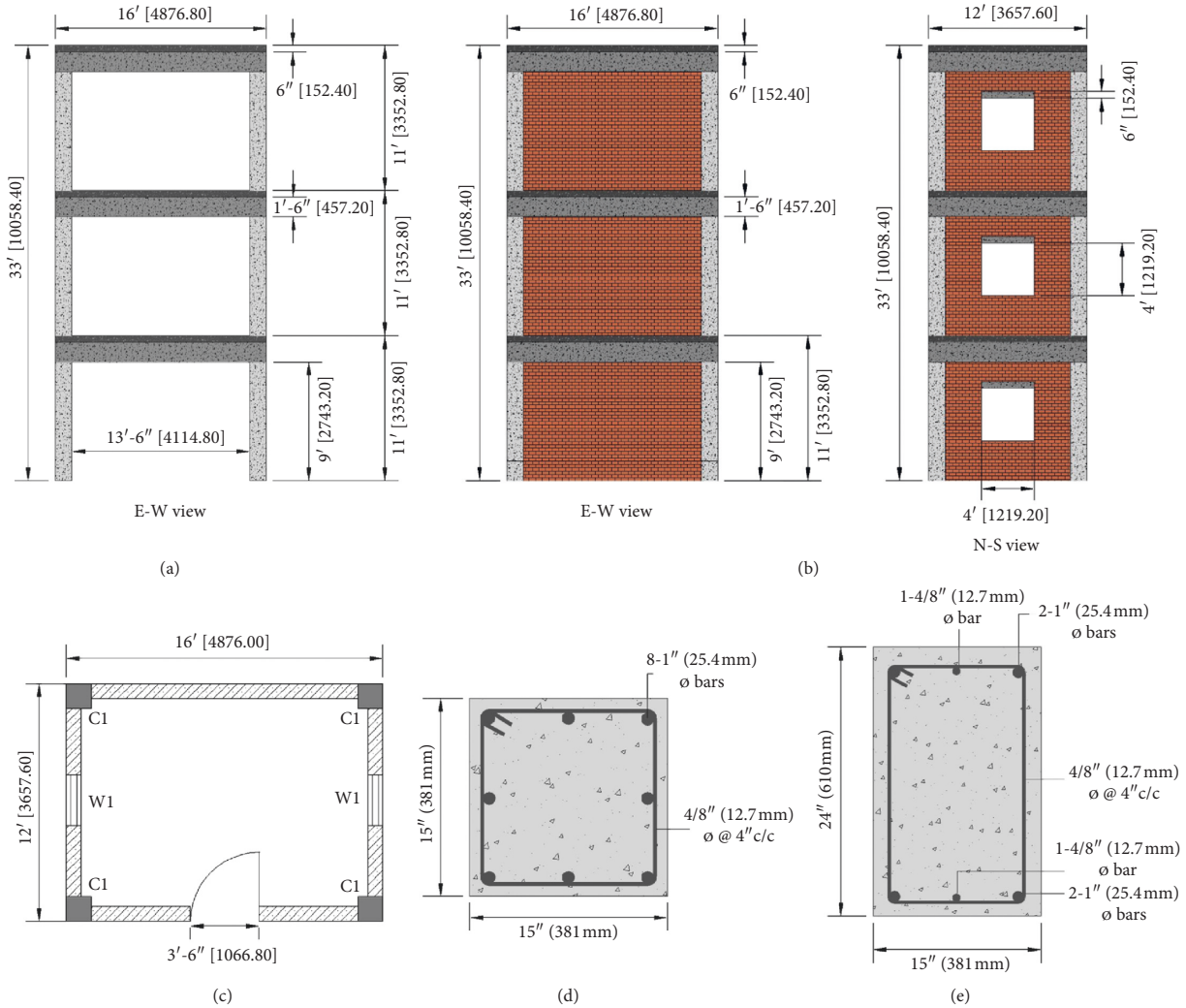

Figure 1: Geometric and reinforcement details of the prototype frames. The dimensions in brackets are given in mm. (a) RC bare frame (b) Masonry-infilled RC frame. (c) Plane view. (d) Column X-section. (e) Beam X-section.

(a) (b)

Figure 2: Brick masonry unit and wallettes used for basic testing of masonry constituents. (a) Masonry wallettes. (b) Brick unit.

The test models were instrumented with accelerometers and displacement transducers at the base and floor levels, in order to record the actual input acceleration time history at the base of the model and floors' acceleration and displacement response (Figure 4).

2.4. Observed Seismic Behavior of Tested Models. Typically, frames conforming to seismic codes have been observed with beam-sway mechanism, i.e., experience flexure yielding at the beam ends and slight flexure cracking at the bottom end of columns at the ground story under input excitation representative of design basis earthquake [24]. Unlike the code-conforming structures, deficient models have been observed with flexure cracking also in columns and severe damages in joint panels under input excitation well below the design-basis earthquake [7, 24]. The use of low-strength concrete and the lack of lateral ties in joint panels, along with improper reinforcement and detailing, have resulted in the

Table 1: Mechanical properties of masonry used for infills in 1 : 4 reduced-scale models.

S. no.	Test	Samples	Properties	Mean value	Std. dev.
1	Compression tests on mortar cubes as per ASTM C-109	6	$f_{m,m}$ (MPa)	12.35	0.45
2	Initial rate of absorption tests on brick masonry units as per ASTM C-67	6	IRA (gm/min/30 in^2)	34.50	7.35
3	Water absorption tests on brick masonry units as per ASTM C-67	6	WA (%)	10.42	1.27
4	Compression tests on brick masonry units as per ASTM C-67	6	$f_{m,b}$ (MPa)	9.87	1.33
5	Compression tests on masonry column prisms as per ASTM C-1314	4	f_m (MPa)	4.22	0.85
6	Compression tests on masonry prisms (305 mm × 305 mm) as per ASTM C-1314	4	f_m (MPa)	4.05	0.17
7(a)	Direct in-plane shear tests on masonry wallettes (305 mm × 305 mm) as per the RILEM specifications	4	T_0 (MPa)	0.36	0.04
7(b)	Direct in-plane shear tests on masonry wallettes (305 mm × 305 mm) as per the RILEM specification	4	f_{tu} (MPa)	0.26	0.03

Table 2: Properties of test models.

Structural properties	
Prototype frame	Test models (scale 1 : 4)
Beams	
15 in × 18 in (381 mm × 457 mm)	3.75 in × 4.5 in (96 mm × 114 mm)
Columns	
15 in × 15 in (381 mm × 381 mm)	3.75 in × 3.75 in (96 mm × 96 mm)
Slab	
6 in (153 mm)	1.5 in (40 mm)
Concrete strength	
3000 psi (21 MPa)	2500 psi (17.24 MPa)
Aggregate size: 1 in	Aggregate size: 3/8 in
Steel strength	
60000 psi (414 MPa)	60000 psi (414 MPa)
#8 rebar (25.40 mm)	#2 rebar (6.35 mm)
#4 rebar (12.70 mm)	#1 rebar (3.18 mm)

Table 3: Model-to-prototype quantity conversion factors.

Simple model similitude requirement		
Physical quantity	Relationship	Scale factor
Length	$S_L = L_p/L_m$	4
Stress	$S_f = f_p/f_m$	1
Strain	$S_\varepsilon = \varepsilon_p/\varepsilon_m$	1
Specific mass	$S_\varepsilon = \varepsilon_p/\varepsilon_m$	1
Displacement	$S_d = d_p/d_m = S_L$	4
Force	$S_F = F_pF_m = S_L^2S_f$	16
Time	$S_t = t_p/t_m = S_L\sqrt{S_\varepsilon S_\rho/S_f}$	$\sqrt{4}$
Frequency	$S_\Omega = \Omega_p/\Omega_m = 1/S_t$	$1/\sqrt{4}$
Velocity	$S_v = v_p/v_m = \sqrt{S_\varepsilon S_\rho/S_f}$	1
Acceleration	$S_a = a_p/a_m = S_f/S_LS_\rho$	1/4

concrete cover spalling and core crushing of joint panels under seismic excitations. The seismic behavior of considered bare and masonry-infilled RC frames is described as follows.

2.4.1. Model 1: Bare RC SMRF Structure. For input excitation of NR1 (i.e., acceleration amplitude 100% of Northridge), the model was observed with few hairline flexure cracks in the columns at the ground and first story. Slight vertical cracks were observed at the ends of the beams of in-plane frames on the first floor. Very few hairline cracks were observed in the joint panels on the first floor. For input excitation of NR2 (i.e., acceleration amplitude 250% of Northridge), further slight-to-moderate cracks appeared in the structure, particularly in the joint panels (Figure 5). Few

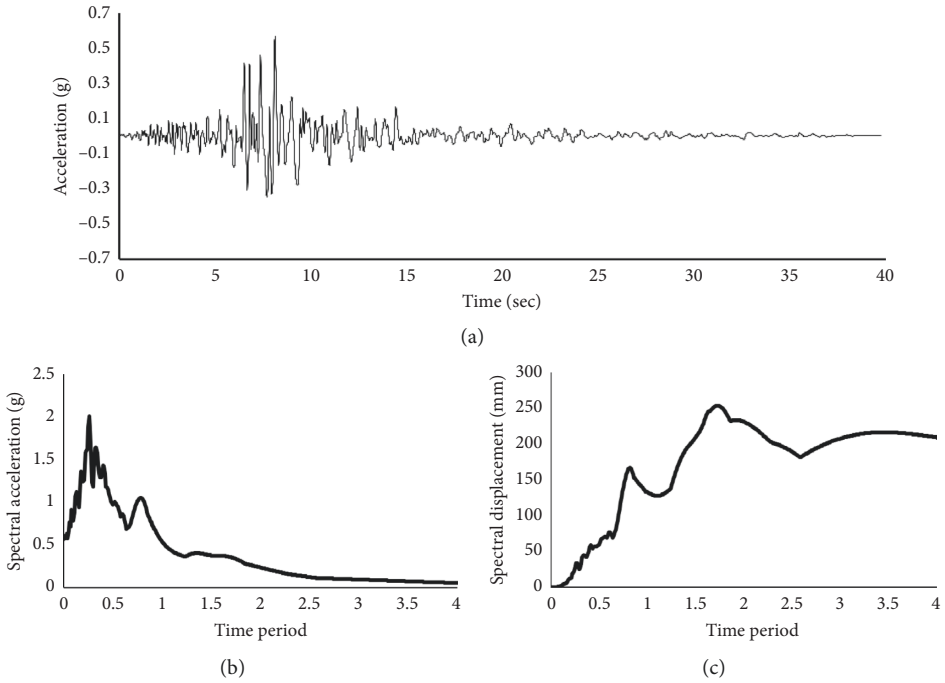

Figure 3: Selected earthquake record for shake table tests. (a) Northridge 1994 acceleration time history. (b) 5% damped acceleration response spectra. (c) 5% damped displacement response spectra.

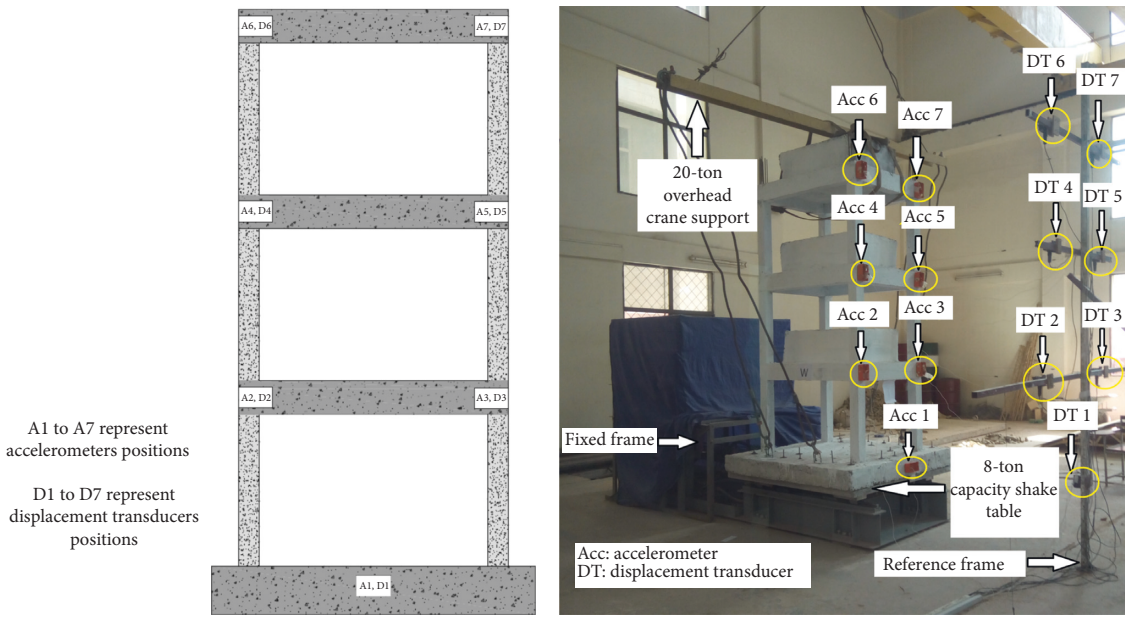

Figure 4: Test model instrumentation plan.

slight cracks also occurred in the joint panels on the second floor. The number and severity of cracks were primarily higher in the joint panels on the first floor, which is due to the fact that the bending and rotation demand are usually higher in beam-column connection at the first floor. Flexure cracks at the top and bottom ends of first-story columns aggravated further. Slight flexure cracks were also observed at the base of columns on the second story. On ground story, slight flexure cracks were observed at the top ends, and very few hairline cracks appeared on the ground-story columns at distance from the bottom ends. The severity of damage in the joint panels is due to the lack of lateral ties in the panels, resulting in joint shear strength lower than the excitation-induced joint shear demand. Following the localized shear damages in joint panels upon the exceedance of principal tensile strength of concrete in joints, global instability and abrupt story mechanism are very likely to result in the catastrophic collapse of the structure [25, 26, 27].

Figure 5: Damages observed in the frame structure under 200% earthquake motions. (a) In-plane loaded frame. (b) Face-loaded frame. (c) Damage to joints on first floor. (d) Damages observed in beams and joints at the second floor. (e) Damage pattern at corners.

The relatively lower damage in beams is suggesting the contribution of slab to the stiffness and strength of beams, thereby forcing columns to undergo inelastic actions. This can be contrasted with the mechanism developed in the counterpart portal frame for the same structure, when the slab contribution is neglected. It is worth to mention that the exterior column depth is 15 times the diameter of longitudinal rebars in beams, indicating the ACI 318 requirements for column depth are not sufficient to avoid flexure inelastic actions in columns and shear damages in joint panels.

2.4.2. Model 2 and Model 3: Masonry-Infilled RC SMRF Structures. For input excitation of NR1, the model was observed with hairline through cracks in in-plane masonry infills having opening for doors. This comprised primarily horizontal cracks at the masonry bed joints. These cracks were observed on all the three stories; however, the severity of cracks was high on ground story, which is due to the higher interstory drift demand at the ground story. Solid in-plane parallel masonry wall panels were observed with horizontal and vertical cracks at the masonry and frame interfaces, causing separation of masonry infill. This was observed only on the ground story. Out-of-plane wall panels having opening for windows were also observed with minor through cracks, propagating from the windows corners. Such damages were observed on all the three stories.

For input excitations of NR2, the existing cracks further aggravated and few additional cracks were also observed (Figure 6). Masonry infill separation has been also observed at the ground story in the in-plane walls having opening for door. Vertical and horizontal cracks also appeared in the parallel in-plane solid masonry infill on both the second and

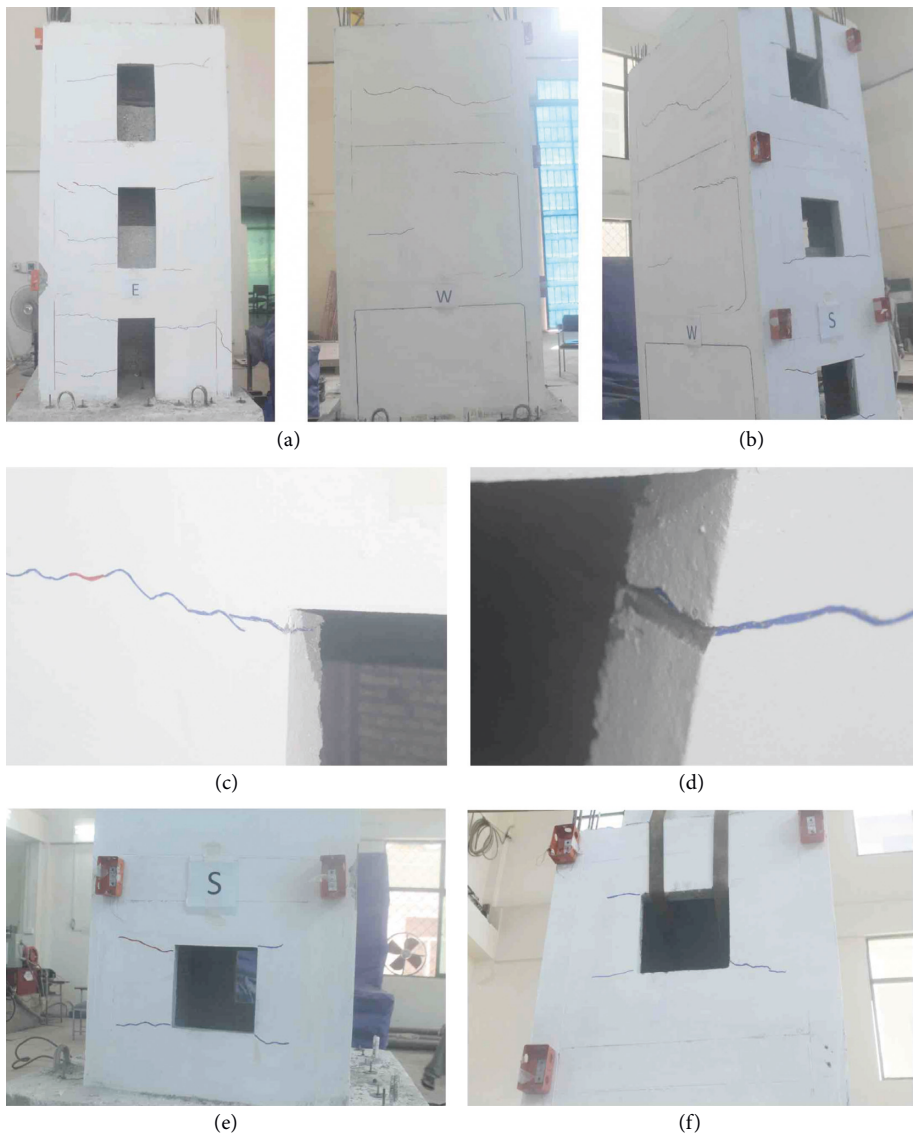

(a) (b) (c) (d) (e) (f)

Figure 6: Damages observed in the hybrid masonry-infilled frame structure under 200% earthquake motions. (a) In-plane loaded frame. (b) Face-loaded frame. (c) Through horizontal cracks in masonry panel. (d) Horizontal sliding at the masonry bed joint. (e) Damage to out-of-plane panel on ground story. (f) Damage to out-of-plane panel on third story.

third stories. The third-story masonry solid wall panel was observed with horizontal cracks. Flexure damages in beams and columns and shear cracks in beam-column joint panels were not observed. It is due to the fact that under later loads, the masonry infill develops diagonal compression strut bearing against the beam and column at distance from the joint panels. Localized opposing shear force is developed in beams and columns at the strut contact at distance from the joint panel. This reduces shear demand on joint panels, due to which the joint panels are not subjected to large shear deformation.

Both the masonry-infilled frames, conventional and hybrid, behaved very much similar. However, the conventional masonry-infilled RC frame was observed with relatively more distributed cracks and panel separation of in-plane walls over all the three stories. No cracking or damage was observed in beams, columns, and joint-panel regions; this shows effectiveness of masonry infill in avoiding joint-panel damage of the bare frame.

3. Elastic Dynamic Properties of Test Structures

3.1. Fundamental Frequency/Time Period. Structural modal frequencies were computed through low-amplitude tests performed on structures through shake table impact (jerk loading) before the actual tests. Roof acceleration response of the model was obtained and analyzed to derive floor acceleration response spectra, in frequency domain, to identify the structural predominant frequency. Figure 7 shows floor spectra developed for bare frame structure under the free-vibration test. The lowest predominant frequency was identified for each model: 3.271 Hz (0.305 sec) for bare frame, 3.418 Hz (0.293 sec) for hybrid masonry-infilled frame, and 3.369 Hz (0.297 sec) for masonry-infilled

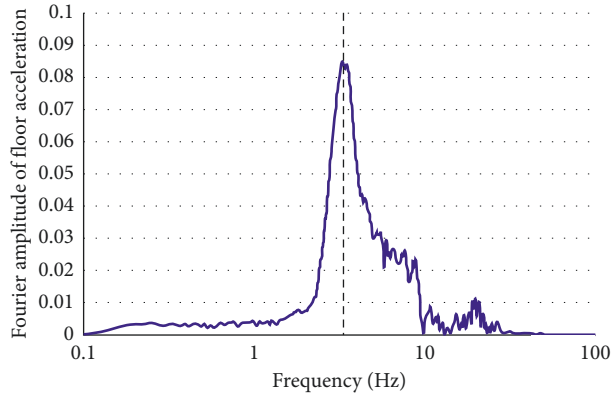

Figure 7: Fourier spectra of floor acceleration response at roof level for free vibration of undamaged bare frame structure. The values are those for the reduced scale test model.

frame reduced scale test models. This corresponds to the prototype time period of 0.61 sec for bare frame, 0.59 sec for hybrid masonry-infilled frame, and 0.59 sec for masonry-infilled frame. As expected, the elastic period of masonry-infilled structure is relatively lower than the bare frame structures. Further, the time period of hybrid masonry-infilled structure is also less than that of the counterpart conventional masonry-infilled structure. It is worth to mention that structural stiffness of masonry-infilled frames increased due to inclusion of masonry infill. However, this also increased the structural mass, and the period variation in bare to masonry-infilled structure is not very significant. It is due to the fact that the frame itself is significantly stiffer, and also, due to the relatively lower bay width-to-height ratio of frame, the frame is mainly governed by the global flexure/rocking frame behavior. For these reasons, the infill does not contribute significantly to the frame stiffness.

The present Building Code of Pakistan [20] has proposed structural height-based equation to calculate the structure period of RC frame:

$$T_a = 0.03h^{3/4}, \quad (1)$$

where T is the fundamental period of structure and h is the total height of structure in feet. The above equation provides an estimate of fundamental period of 0.41 sec for prototype of bare frame, which is about 50% lower than the measured structural period. Similar discrepancy between calculated and observed time period of reinforced concrete structures has been observed in many other studies [28, 29]. The code also allows a 30% increase in the time period of structure calculated using equation (1), as the actual model analysis of structure may give higher value for time period. Considering this increase, the time period will increase to 0.54 sec for bare frame. Therefore, the discrepancy in calculated and measured time period reduces to about 12%. Furthermore, the fact that simplified formulation provided by codes provides underestimating estimates of the vibration period of structures is somehow expected, given that such underestimation is usually conservative within a force-based approach to seismic design.

3.2. Elastic Viscous Damping. The decay function for the time history response as proposed by Chopra [30] was used to calculate the test model damping:

$$\zeta = \frac{1}{2n\pi} Ln\left(\frac{A_1}{A_n}\right), \quad (2)$$

where ζ represents the elastic damping coefficient; A_1 represents the peak amplitude of response displacement at reference point 1; A_n represents the peak amplitude of response displacement at reference point after n cycles; and n represents the number of cycles between the peaks. The model damping was calculated from the free vibration tests conducted on models, carried out by means of shake table jerk loading. The structure displacement response at the top was considered and analyzed for calculating the decay in the displacement history (Figure 8). The damping was calculated from logarithmic decay of the last two cycles. The structural damping measured herein is 10.57% for bare frame, 13.36% for hybrid masonry-infilled frame, and 13.73% for masonry-infilled frame. The measured elastic damping can be contrasted with the normally proposed 5% elastic damping.

4. Observed Seismic Response of Test Structures

4.1. Acceleration-Displacement Response Spectrum of Input Excitations. To analytically compute the acceleration and displacement demands on the hypothetical elastic structure, acceleration-displacement response spectrum (ADRS) were developed for each tests by taking recorded accelerations time history at the base of the models. The elastic peak acceleration and displacement demand on hypothetical structure may be read at the intersection on the ADRS drawing a radial line whose slope is equal to the square of the circular frequency of the structure for the first mode vibration period (see Figure 9). As typical for the elastic response analysis, 5% viscous damping is normally considered for the elastic analysis of structures. Although the acceleration time history of 1994 Northridge earthquake has been used for all the three models, the actual recorded input excitations of all the test models differ to some extent. It is worth mentioning that the input to the shake table controller was the same in all cases; however, the controller develops

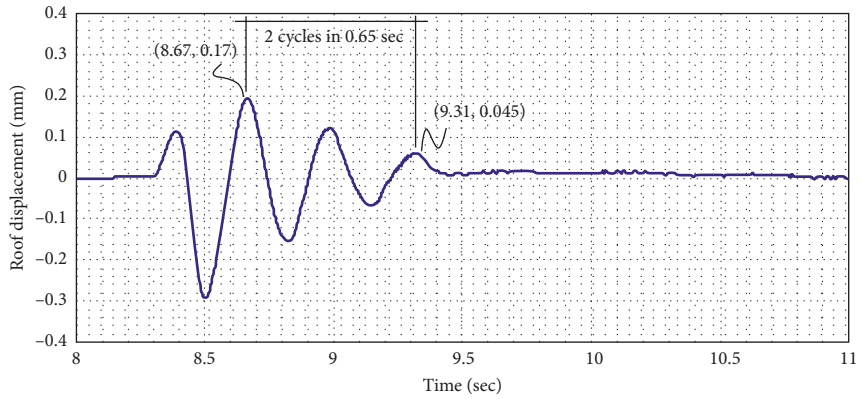

Figure 8: Top-floor displacement response of undamaged bare frame structure for the free vibration test. The values are those for the reduced scale test model.

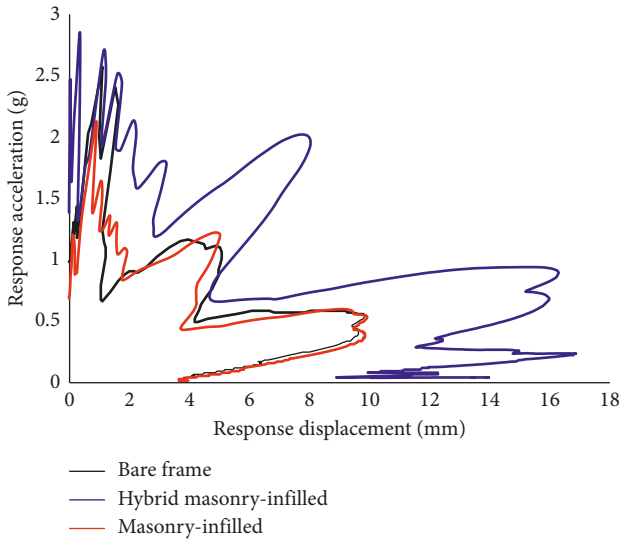

Figure 9: Acceleration-displacement response spectrum for recorded input excitation at the base of test models under 100% (NR1) of earthquake motions.

different auto transfer function in all structure cases. Although this depends on the test model stiffness and masses, uncertainties may be encountered due to the automatic control system of controller and the differences the controller face in the current hydraulic pressure and temperature. The latter cannot be maintained exactly the same in all cases.

4.2. Interstory Drift, Lateral Displacement, and Interstory Shear Demands. Floor response acceleration and response displacements recorded for each tests were analyzed to obtain the interstory drift profile (Figure 10), lateral floor displacement peak response envelope (Figure 11), and interstory shear (Figure 12). The story shear was calculated based on the equilibrium consideration and by summing the floor inertial forces. The inertial forces at floor levels were the total inertial forces calculated by multiplying the floor absolute acceleration with the lumped mass. The absolute acceleration was measured through 1-DOF accelerometers. Under NR1, the bare frame has experienced interstory drift demand of about 0.89%, which has been reduced by 77% and 80% for the hybrid and conventional masonry-infilled frame, respectively. Similarly, under NR2, the bare frame has experienced interstory drift demand of about 1.63%, which has been reduced by about 74% for the hybrid and conventional masonry-infilled structures, respectively. The infilled structures have controlled the seismic drift demand, largely, because of their relatively high structural stiffness, and also, because of structural energy dissipation capability.

The later can be explained by realizing the occurrence of higher number of cracks experienced in conventional masonry-infilled structures, thereby providing sources for energy dissipation through friction sliding. The masonry panels separation in conventional masonry-infilled structure at all floors allowed the structure to linearly distribute lateral seismic displacement demand on structure, as evidenced from the linear deflected shape of masonry-infilled structure (Figure 10). On the contrary, relatively high stiffness of masonry-infilled RC structures attracted higher

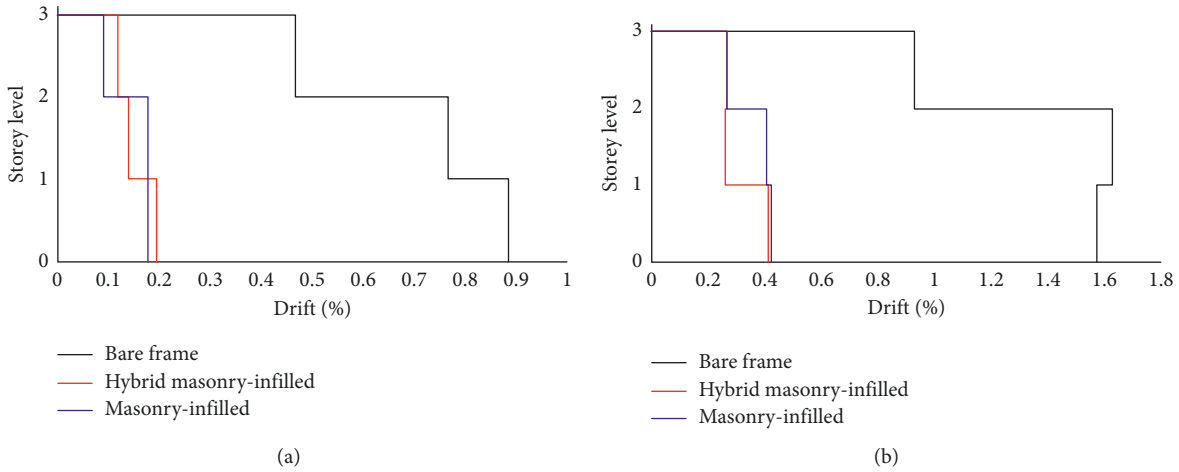

Figure 10: Maximum interstory drift envelope of test models for increasing input excitation. (a) Interstory drift demand under NR1. (b) Interstory drift demand under NR2.

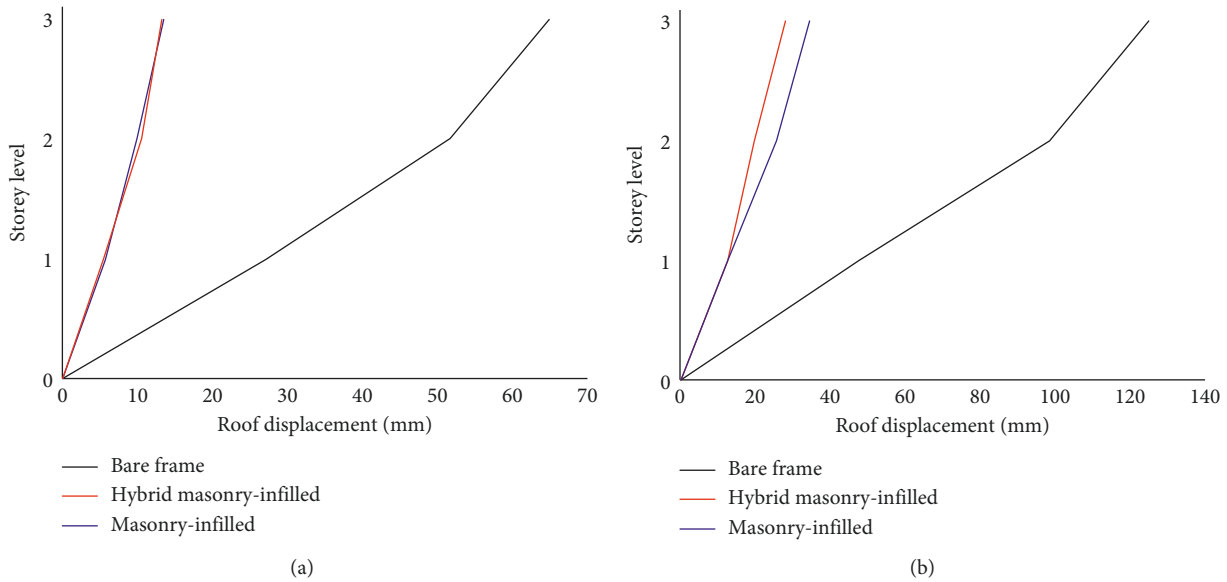

Figure 11: Maximum lateral displacement envelope of test models for increasing input excitation. Displacements were converted to the corresponding prototype values. (a) Lateral displacement under NR1. (b) Lateral displacement under NR2.

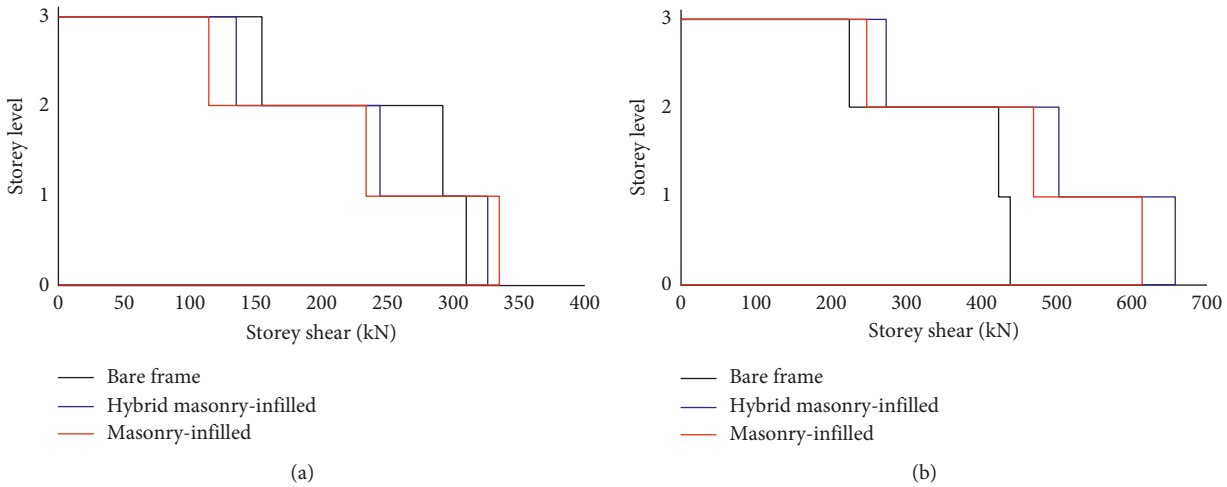

Figure 12: Maximum interstory shear envelope of test structures for increasing input excitation. Story shears were converted to the corresponding prototype values. (a) Interstory shear under NR1. (b) Interstory shear under NR2.

base shear force. Under NR1, both the masonry-infilled structures attracted similar base shear force with marginal difference, which increases under higher input excitation.

4.3. Floor Acceleration Amplification. The model amplification was measured dividing the structural peak response acceleration at the top floor over the peak input acceleration at the base of the model:

$$\text{Amp} = \left(\frac{\max A_{\text{roof}}}{\max A_{\text{base}}}\right), \tag{3}$$

where Amp represents the top floor acceleration amplification factor; $\max A_{\text{roof}}$ represents the peak acceleration observed at the roof level; and $\max A_{\text{base}}$ represents the peak acceleration of earthquake motions observed at the base of the model.

The measured amplification initially increased with increasing intensity that suggests a direct correlation between the intensity and the acceleration amplification (Figure 13). However, the amplification started decreasing with further increase in input base excitation that highlights the onset of cracking/damage in structures. This is also evident from the hysteretic response and cumulative energy dissipation of test models (Figures 14 and 15). The occurrence of cracking and damage provided energy dissipation capacity; due to this, the structures' peak response accelerations were reduced. The maximum acceleration amplification observed in the bare frame is 3.10, which is reduced to 2.60 and 2.47 in case of hybrid masonry-infilled and masonry-infilled structures, respectively. As expected, the floor acceleration amplification was reduced in case of masonry-infilled structures, which was due to the relatively higher structural damping available in these structures, provided by masonry panel-frame interaction (vertical and horizontal cracks at infill-frame interfaces) and masonry friction sliding observed at the masonry bed joint in cracked/damaged infill.

4.4. Seismic Response Curves. The peak-observed input accelerations, expressed as PGA, were correlated with the roof displacement demand to derive seismic response curves for test models (Figure 16). These curves show the structural lateral deformation against the input excitations. As can be seen, initially, the curves behave linearly but deviate due to onset of structural damages and tend to flatten for extreme level shaking (e.g., in case of bare frame).

The later corresponds to the development of nonlinearity in the structural system due to cracking/damage. A minor deviation in the response curve of masonry-infilled frames is due to the cracking/damages observed in masonry infill. On the other hand, a large deviation has been observed in the response curve for bare frame, which was due to the shear damages observed in joint panels. These joint panel damages allowed the structure to deform to larger lateral displacement under relatively lower input excitations. It can be observed that both the masonry-infilled structures increased the structural resistance against the input excitation, thereby making the structure

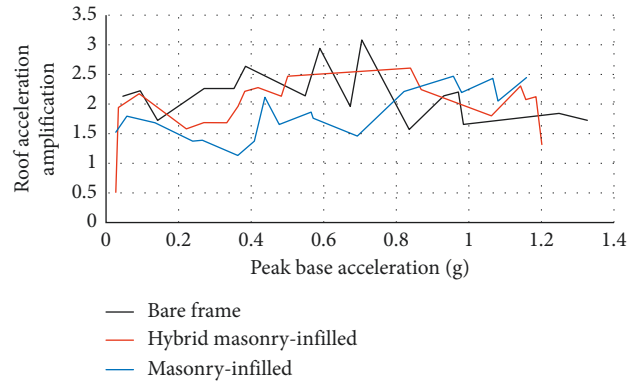

Figure 13: Acceleration amplification of structures correlated with input excitation peak acceleration. The values are those for the reduced scale test model.

able to resist higher peak input acceleration. Furthermore, the inclusion of masonry infill enabled the structure to control lateral deformation under earthquake ground motions, which was primarily due to the relatively high stiffness of the masonry-infilled structures, and by larger part, it was due to the characteristics of the damaged masonry-infills that provided energy dissipation through masonry sliding over multiple cracks.

5. Seismic Performance Assessment of Test Models

5.1. Seismic Analysis of Test Models Using Static Force Procedure

5.1.1. Measured Mode Shapes and Participation Factors. The estimation of elastic base shear requires the identification of deflected shape of structure and participation factor for the first mode of vibration, which is inferred from the measured lateral floor displacement of the tested models. A structural node can have 6 degrees-of-freedom for deformation; however, lateral horizontal translation of floors is the predominant deformation of frame structures for structural vibration under seismic excitation. Thus, a simple three-degrees-of-freedom system with lumped masses at the floor was used to express the lateral response of the tested models. The lumped weights associated with each of the three floors of test models were equal to, from third to first story, [0.625 0.655 0.655] and [0.725 0.855 0.855] for the bare frame and masonry-infill model, respectively. Since structural displacements during lateral vibration are generally larger at the first mode, the coordinates of deflected shape were determined by normalizing measured lateral floor displacements of the structure at times of peak response with respect to the roof floor. First-mode participation factors were determined from the modal coordinates and floor weights in accordance with equation (4), which are given in Table 4:

$$\Gamma_1 = \frac{\sum_{i=1}^{m} w_i \phi_{1i}}{\sum_{i=1}^{m} w_i \phi_{1i}^2}, \tag{4}$$

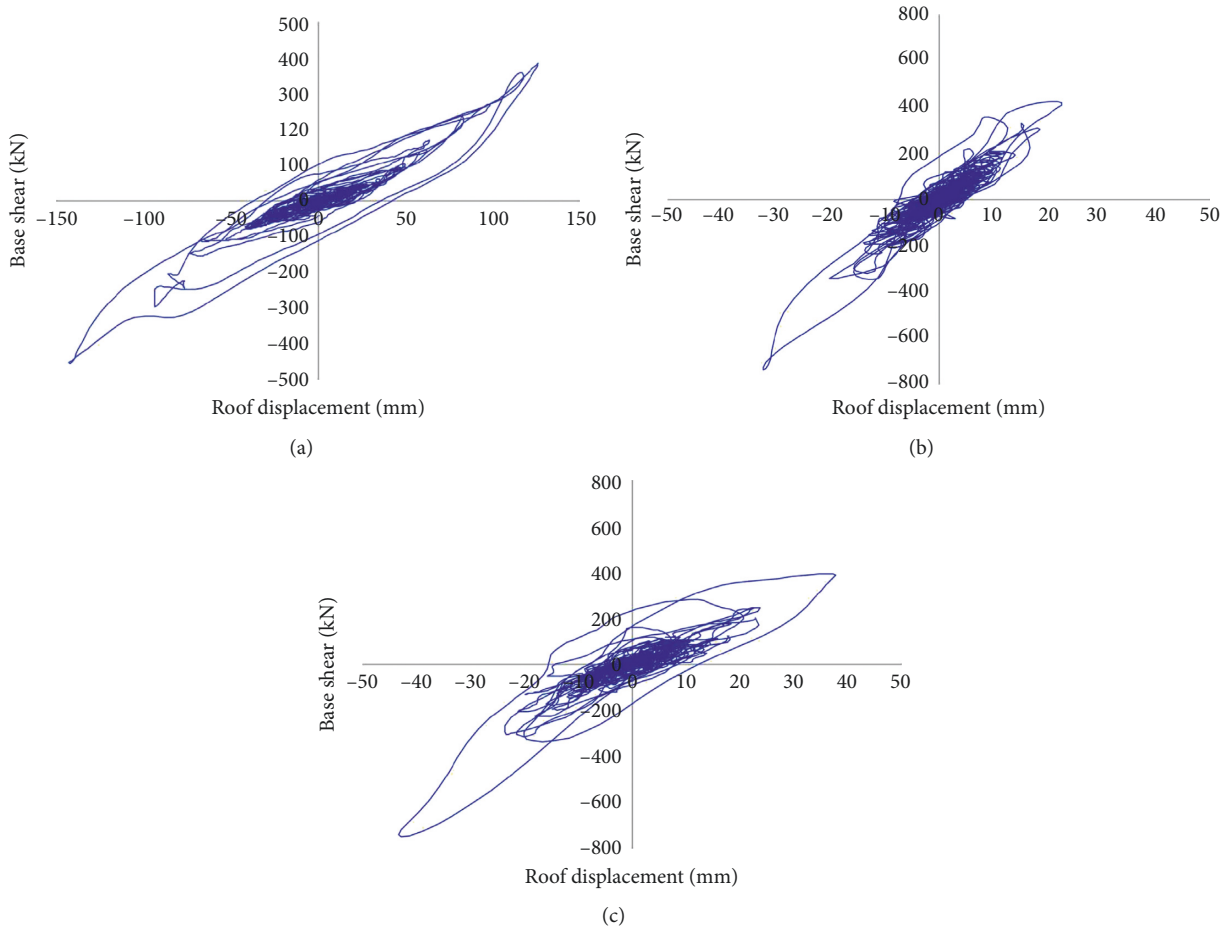

Figure 14: Measured force-displacement hysteretic response of the prototype of test models for NR2. (a) Bare frame. (b) Hybrid masonry-infilled. (c) Masonry-infilled.

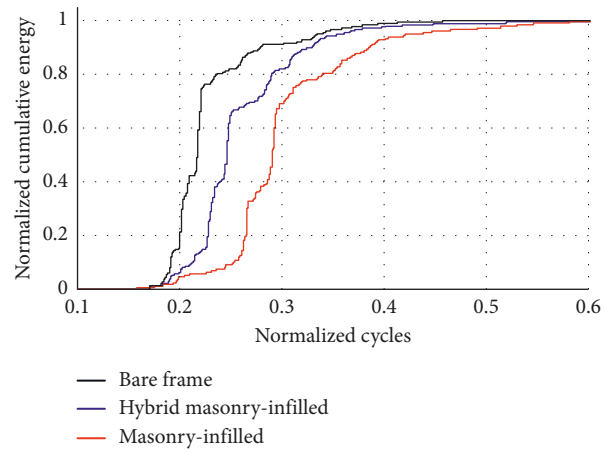

Figure 15: Normalized cumulative energy dissipation of test structures under NR2. A curve with more flatness signifies higher energy dissipation.

where w_i is the floor weight, ϕ_1 represents the coordinates of mode shape, and i is the floor level. The calculated participation factor was used to determine the percentage of the total weight effective in the first mode of the structure, in accordance with equation (5), and is given in Table 4.

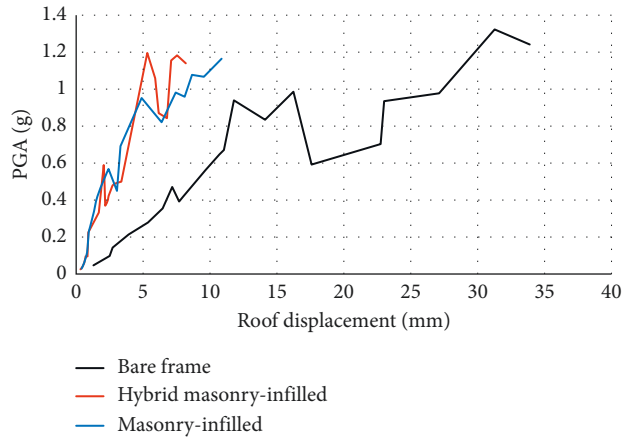

Figure 16: Seismic response curves developed for the prototype of test models.

Table 4: Base shear force demands for models calculated from the 5% damped elastic acceleration spectrum generated for input acceleration.

Model	Test run	Frequency (Hz)	S_a (g)	Γ_1	$W_{effective}$ (%)	V_{b1} (kN)*	Diff. (%)
Bare frame	BF_NR1	3.08	0.91	1.23	90.19	249	−19.68
	BF_NR2	2.73	1.94	1.22	89.69	528	20.27
Hybrid masonry infill	HM_NR1	3.37	0.71	1.28	90.69	246	−24.54
	HM_NR2	3.32	1.36	1.31	89.22	464	−29.48
Masonry infill	CM_NR1	3.32	0.85	1.25	89.72	291	−13.13
	CM_NR2	3.13	1.23	1.25	88.85	418	−31.81

*The values were converted to the corresponding prototype structures using the applicable scaling factors.

$$W_{\text{effective}}(\%) = \frac{\Gamma_1 \sum_{i=1}^{m} w_i \phi_{1i}}{W} \times 100. \quad (5)$$

The percentage of the total weight of structure that is effective in the first mode ranged from about 88.85% to 90.69% and is higher for the first test runs. This is because, for the first test runs, the deflected shape was more linear, and thus, lateral floor displacements were higher.

5.1.2. Base Shear Force. The elastic base shear demand for a specified mode is related to the spectral acceleration S_a, which is calculated in accordance with the following equation:

$$V_{b1} = \Gamma_1 \frac{S_{a1}}{g} \sum_{i=1}^{m} w_i \phi_{1i}, \quad (6)$$

where V_{b1} is the elastic base shear demand for first mode and S_{a1} is the spectral acceleration demand on the hypothetical elastic model, obtained from the elastic acceleration spectrum at the fundamental time period of the test models obtained through free vibration tests. Thus, base shear demand of a hypothetical linearly behaving system was deduced, which is given in Table 4. Table 4 also reports the difference observed between the analytically predicted and experimentally observed base shear force. The negative value indicates underprediction, and the positive value indicates overprediction. The difference between the actual and analytically computed base shear is relatively less in case of NR1 but increased in case of NR2. It is due to the fact that under higher seismic excitations, the onset of structural nonlinearity makes the analytical prediction less accurate. The base shear force calculated analytically is less in all cases, which seems to be due to the approximations made, i.e., considering only Mode 1 for computation and idealizing model vibration period based on the free vibration tests. The base shear force calculated analytically for bare frame in case of NR2 is higher than the actually observed. It is due to the fact that under NR2 the bare frame was subjected to significant nonlinearity, whereby the static procedure that assumes linear behavior becomes less accurate and overpredicts base shear force.

5.2. Seismic Fragility Functions. Seismic fragility functions are a set of mathematical cumulative distribution functions that describe structural damages probabilistically in terms of the performance level exceedance of structure, given the input excitation. It is derived using standard normal cumulative distribution functions, as formulated [31]:

$$P_{LS} = \Phi\left(\frac{1}{\beta} Ln\left(\frac{\text{PGA}}{\text{pga}_{LS}}\right)\right), \quad (7)$$

where P_{LS} is the probability of exceedance of a given limit state, Φ is the standard normal cumulative distribution mathematical function, PGA is the specified peak ground acceleration demand, pga_{LS} is the peak ground acceleration corresponding to ground motions capable of exceeding the structure specified drift level by 50%, and β is the logarithmic

Table 5: PGA_{LS} derived for roof drift of 0.30%.

Performance levels	Mean values of PGA, pga_{LS}	Log. standard deviation β
Bare frame	0.45	0.60
Hybrid masonry-infill	1.16	0.60
Masonry-infill	1.05	0.60

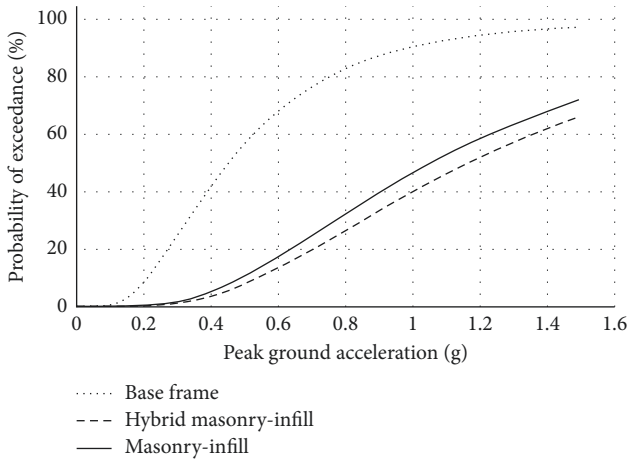

Figure 17: Seismic fragility functions derived for probabilistic assessment of test models. The functions are derived for a roof drift of 0.30%.

standard deviation that defines total uncertainties. Derivation of fragility functions for a structure requires pga_{LS} and β for each limit state. The value of β varies from 0.40 to 0.60 [32, 33], $\beta = 0.60$ was taken in the present case. For the present building, pga_{LS} was obtained from the seismic response curves (Figure 16). Since, the masonry-infill structure were laterally displaced to only 0.30% roof drift, roof drift of 0.30% was taken as the reference roof drift for which the corresponding PGAs were obtained through second-order polynomial interpolation. These values were considered as the mean estimate of pga_{LS} and listed in Table 5. Fragility functions derived using equation (7) are reported in Figure 17. Considering the 10% probability of exceedance for the specified roof drift of 0.30%, the bare frame will resist 0.21 g, hybrid masonry-infill frame will resist 0.54 g, and conventional masonry-infill will resist 0.50 g. The use of masonry infill (i.e., hybrid and conventional) increased the seismic resistance of the bare frame by 157% and 133%, respectively. Both the hybrid and conventional masonry-infill frames resulted in similar fragility functions; however, the hybrid masonry-infill frame has relatively more resistance in comparison to conventional masonry infill.

The indicated input excitation has 50% probability to exceed the specified roof drift of 0.30%.

6. Conclusions

Shake table tests were performed on three 1 : 4 reduced-scale three-story reinforced concrete frames, with and without masonry infill, representative of modern frame structures found in most of the developing countries, possessing construction deficiencies like lack of ties in joint panels and concrete having low strength. The models were tested using natural acceleration time history of 1994 Northridge, with multilevel excitations. Additionally, free vibration shake table impact (jerk) tests were conducted. Seismic behavior of the test models was observed, and fundamental dynamic properties and seismic response parameters were obtained. The seismic response of bare frame and masonry-infill frames were critically compared. The seismic performance of test models was assessed using static force procedure and probabilistic fragility functions.

The lack of lateral ties in beam-column joint panels in SMRF structures resulted in the local shear damage of joint panels. The SMRF structure, with structural members detailed as per the ACI-318-05 but lacking confining ties in the joint panel region, has revealed significant damages in joint panel regions of bare frames under earthquake motions. These damages, if experienced under moderate ground motions, create challenges in routine repairing. The inclusion of masonry infill, either through a conventional masonry-infilled construction or hybrid masonry-infill construction, has avoided damages in the joint panel region by altering lateral load path and controlling lateral displacement demands on structures through energy dissipation offered by masonry sliding observed at multiple cracks. Through the infill-frame interaction, conventional masonry-infill RC structure offered more energy dissipation as compared to hybrid masonry-infilled RC structures. The same has been manifested in the probabilistic fragility functions developed for the test models for a target roof drift, which has revealed that the masonry infill has enhanced the seismic resistance of structures by 133% to 157% using conventional and hybrid masonry infill, respectively.

Data Availability

The related dataset can be provided by contact at naveed.ahmad@uetpeshawar.edu.pk.

Disclosure

The research work presented herein is based on the final year projects of senior undergraduate students in the Department of Civil Engineering of UET Peshawar.

Conflicts of Interest

The authors declare that they have no conflicts of interest.

References

[1] M. H. Arslan and H. H. Korkmaz, "What is to be learned from damage and failure of reinforced concrete structures during

recent earthquakes in Turkey?," *Engineering Failure Analysis*, vol. 14, no. 1, pp. 1–22, 2007.

[2] S. Ates, V. Kahya, M. Yurdakul, and S. Adanur, "Damages on reinforced concrete buildings due to consecutive earthquakes in Van," *Soil Dynamics and Earthquake Engineering*, vol. 53, pp. 109–118, 2013.

[3] J. K. Bothara and K. M. O. Hicyilmas, "General observations of building behavior during the 8th october 2005 Pakistan earthquake," *Bulletin of the New Zealand Society for Earthquake Engineering*, vol. 41, no. 4, pp. 209–233, 2008.

[4] B. Erdil, "Why RC buildings failed in the 2011 Van, Turkey, earthquakes: construction versus design practices," *Journal of Performance of Constructed Facilities*, vol. 31, no. 3, Article ID 04016110, 2016.

[5] T. Rossetto and N. Peiris, "Observations of damage due to the Kashmir earthquake of october 8, 2005 and study of current seismic provisions for buildings in Pakistan," *Bulletin of Earthquake Engineering*, vol. 7, no. 3, pp. 681–699, 2009.

[6] J. G. Ruiz-Pinilla, J. M. Adam, R. Pérez-Cárcel, J. Yuste, and J. J. Moragues, "Learning from RC building structures damaged by the earthquake in Lorca, Spain, in 2011," *Engineering Failure Analysis*, vol. 68, pp. 76–86, 2016.

[7] N. Ahmad, A. Shahzad, M. Rizwan et al., "Seismic performance assessment of non-compliant SMRF-reinforced concrete frame: shake-table test study," *Journal of Earthquake Engineering*, vol. 23, no. 3, pp. 444–462, 2019.

[8] N. Ahmad, J. Akbar, M. Rizwan, B. Alam, A. N. Khan, and A. Lateef, "Haunch retrofitting technique for seismic upgrading deficient RC frames," *Bulletin of Earthquake Engineering*, vol. 17, no. 7, pp. 3895–3932, 2019.

[9] J. Akbar, N. Ahmad, and B. Alam, "Seismic strengthening of deficient RC frames using reinforced concrete haunch," *ACI Structural Journal*, vol. 166, no. 1, pp. 225–235, 2019.

[10] J. Akbar, N. Ahmad, and B. Alam, "Seismic performance of RC frames retrofitted with haunch technique," *Structural Engineering and Mechanics*, vol. 67, no. 1, pp. 1–8, 2018.

[11] M. Banazadeh, M. Gholhaki, and H. Parvini Sani, "Cost-benefit analysis of seismic-isolated structures with viscous damper based on loss estimation," *Structure and Infrastructure Engineering*, vol. 13, no. 8, pp. 1045–1055, 2017.

[12] A. Benavent-Climent, L. Morillas, and D. Escolano-Margarit, "Seismic performance and damage evaluation of a reinforced concrete frame with hysteretic dampers through shake-table tests," *Earthquake Engineering & Structural Dynamics*, vol. 43, no. 15, pp. 2399–2417, 2014.

[13] F. Bencardion, A. Condello, and F. Castiglione, "An innovative solution for the structural consolidation of RC modern cultural heritage," *International Journal of Architectural Heritage*, vol. 11, no. 6, pp. 829–842, 2017.

[14] M. Dolce, D. Cardone, F. C. Ponzo, and C. Valente, "Shaking table tests on reinforced concrete frames without and with passive control systems," *Earthquake Engineering & Structural Dynamics*, vol. 34, no. 14, pp. 1687–1717, 2005.

[15] R. Marques, P. Lamego, P. B. Lourenci, and M. L. Sousa, "Efficiency and cost-benefit analysis of seismic strengthening techniques for old residential buildings in Lisbon," *Journal of Earthquake Engineering*, vol. 22, no. 9, 2018.

[16] E. Oliver-Saiz and A. Benavent-Climent, "Shake-table test of a reinforced concrete frame retrofitted with hysteretic damper connected using an improved joint structure," in *Proceedings of the Second European Conference on Earthquake Engineering and Seismology*, Istanbul, Turkey, August 2014.

[17] S. I. Pardalopoulos, S. J. Pantazopoulou, and G. E. Thermou, "Seismic rehabilitation of substandard RC buildings with masonry infills," *Journal of Earthquake Engineering*, pp. 1–30, 2018.

[18] A. Sharma, G. R. Reddy, R. Eligehausen, G. Genesio, and S. Pampanin, "Seismic response of reinforced concrete frames with haunch retrofit solution," *ACI Structural Journal*, vol. 111, no. 3, pp. 673–684, 2014.

[19] A. Sharma, G. R. Reddy, and K. K. Vaze, "Shake table tests on a non-seismically detailed RC frame structure," *Structural Engineering and Mechanics*, vol. 41, no. 1, pp. 1–24, 2012.

[20] BCP, *Building Code of Pakistan: Seismic Provisions-2007*, Technical Report, Ministry of Housing and Works, Islamabad, Pakistan, 2007.

[21] ACI-318, *Building Code Requirements for Structural Concrete-ACI 318-05*, American Concrete Institute, Farmington Hills, MI, USA, 2005.

[22] ETABS, *Structural Software for Building Analysis and Design—ETABS*, Computer and Structures Inc. (CSI), Walnut Creek, CA, USA, 2009.

[23] Y. I. Badrashi, Q. Ali, M. Ashraf, and M. Rashid, "Seismic design characterization of RC special moment resisting frames in Pakistan—field survey to laboratory experiments," *Journal of Engineering and Applied Sciences*, vol. 35, no. 2, pp. 25–32, 2016.

[24] M. Rizwan, N. Ahmad, and A. N. Khan, "Seismic performance of compliant and noncompliant special moment-resisting reinforced concrete frames," *ACI Structural Journal*, vol. 115, no. 4, pp. 1063–1073, 2018.

[25] G. M. Calvi, G. Magenes, and S. Pampanin, "Experimental test on a three story RC frame designed for gravity only," in *Proceedings of the 12th European Conference on Earthquake Engineering*, London, UK, September 2002.

[26] R. Park, "A summary of results of simulated seismic load tests on reinforced concrete beam-column joints, beam and columns with substandard reinforcing details," *Journal of Earthquake Engineering*, vol. 6, no. 2, pp. 147–174, 2001.

[27] M. J. N. Priestley, "Displacement-based seismic assessment of reinforced concrete buildings," *Journal of Earthquake Engineering*, vol. 1, no. 1, pp. 157–192, 1997.

[28] H. Crowley and R. Pinho, "Period-height relationship for existing European reinforced concrete buildings," *Journal of Earthquake Engineering*, vol. 8, no. 1, pp. 93–119, 2004.

[29] A. Shing and M. Vona, "Experimental and numerical evaluation of the fundamental period of undamaged and damaged RC framed buildings," *Bulletin of Earthquake Engineering*, vol. 8, no. 3, pp. 643–656, 2010.

[30] A. K. Chopra, *Dynamics of Structures: Theory and Applications to Earthquake Engineering*, Prentice-Hall, Upper Saddle Rive, NJ, USA, 3rd edition, 2003.

[31] C. A. Kircher, A. A. Nassar, O. Kustu, and W. T. Holmes, "Development of building damage functions for earthquake loss estimation," *Earthquake Spectra*, vol. 13, no. 4, pp. 663–682, 1997.

[32] J. K. Bothara, R. P. Dhakal, and J. B. Mander, "Seismic performance of an unreinforced masonry building: an experimental investigation," *Earthquake Engineering and Structural Dynamics*, vol. 39, no. 1, pp. 45–68, 2009.

[33] FEMA, *Multi-hazard Loss Estimation Methodology, Earthquake Model, HAZUS-MH 2.1: Technical Manual*, Federal Emergency Management Agency (FEMA), Washington, DC, USA, 2003.